SPIRE-RAL-PUB-001696

The Imaging FTS for Herschel SPIRE

Bruce. M. Swinyard[*a], Kjetil Dohlen[b], Didier Ferand[b], Jean-Paul Baluteau[b], Dominique Pouliquen[b], , Pascal Dargent[b], Guy Michel[c], Jerome Martignac[d], Peter Ade[e], Peter Hargrave[e], Matthew Griffin[e], Donald Jennings[f], Martin Caldwell[a].

[a]Rutherford Appleton Laboratory, Chilton, Didcot, Oxon, OX11 0QX, U.K.
[b]Laboratoire d'Astrophysique de Marseille, BP 8 13376, Marseille, France,
[c]Observatoire de Meudon, 5 Place Jules Janssen, 92195, Meudon Cedex, Paris, France,
[d]CEA-Service d'Astrophysique, Bât. 709, Orme des Merisiers, 91191 Gif sur Yvette, France.
[e]Department of Physics and Astronomy, Cardiff University, Cardiff, CF24 3YB, U.K.
[f]Goddard Space Flight Center, Greenbelt, MD, 20771, U.S.A,

ABSTRACT

The design of the Fourier Transform Spectrometer for the Herschel sub-millimetre Spectral and Photometric Imaging Receiver (SPIRE) is described. This is an innovative design for a sub-millimetre spectrometer as it uses intensity beam splitters in a Mach-Zehnder configuration rather than the traditional polarising beam splitters. The instrument is required to have a resolution of 0.04 cm^{-1}; have a relatively large field of view (2.6 arcmin circular) and cover a large wavelength range - 200 to 670 microns. These performance requirements lay stringent requirements on all aspects of the design. The details of the optical; mechanical and electrical implementation of the instrument are discussed in the light of the science and engineering requirements and laboratory testing on development models of the mechanism and control system are reported.

Keywords: Instrumentation, far infrared, spectrographs, Fourier Transform Spectrometer, space

1. INTRODUCTION

The ESA Herschel mission[1] (formerly the FIRST mission) is dedicated to observing the cosmos at wavelengths from 85 to 700 μm. It consists of a 3.5 m telescope at a temperature of 80 K with a suite of focal plane instruments cooled to <11 K in a liquid helium cryostat. The SPIRE instrument[2] is one of the three focal plane instruments for Herschel. It will make observations in the 200 to 670 μm band using bolometer detectors. The focal plane unit of SPIRE is operated at cryogenic temperature (<11 K) and the NTD Germanium bolometer feedhorn arrays[3] are operated at ~300 mK. This temperature is provided by a ^{3}He sorption cooler. The instrument has two sub-instruments: a multi-frequency imaging photometer using three separate bolometer arrays with resolving power of about $\lambda/\Delta\lambda \sim 3$, and an imaging Fourier Transform Spectrometer (FTS) that provides a maximum resolving power of 1000 at 250 μm.

The photometer will simultaneously image a 4x8 arcmin field of view onto spectral bands nominally centred on 250, 350 and 500 μm. A beam steering mirror will be used to move or spatially modulate the source image at the detector arrays. The feedhorn arrays do not give instantaneous Nyquist sampling of the sky. Therefore in order to completely spatially sample of the field of view, the image needs to be sequentially stepped by fractions of the Airy pattern diameter using the beam steering mirror. The spectrometer uses two bolometer arrays to give spectrally resolved images of a small (~2.6 arcmin) area of sky with a spectral resolution variable between R~20 to R=1000 at 50 cm^{-1}. The two spectrometer arrays have nominal optical bands of 200-300 and 300-670 μm. The spectrometer shares the input optics of the instrument with the photometer, including the beam steering mechanism.

In a previous paper[4] we discussed the selection of the spectrometer type for SPIRE; gave details of the basic optical design and discussed the prototype mechanism for the mirror movement and the operational characteristics of the instrument. Other papers[5,6] have discussed the overall optical design for SPIRE and the diffraction limited performance of the optics. In this paper we update the description of the design of the spectrometer in section 2; describe in more detail the component parts of the flight design in section 3 and go on to describe prototype bench testing and subsequent performance modelling in sections 4 and 5 respectively.

[*] contact for more information and pre-prints: B.M.Swinyard@rl.ac.uk

2. THE SPIRE FTS

The outline optical configuration is shown in figure 1 and the design as implemented in the SPIRE instrument in figure 2. We give here an updated outline description of the optical design, the detailed optical design is discussed in reference 5. After reflection from the common input mirrors, the spectrometer beam is picked off by a mirror placed at an intermediate field image and sent out of the plane of the photometer system and through the common optical bench. A flat fold mirror redirects it into a parallel plane, separated by 170 mm from the photometer plane. The input relay mirror focuses the beam to an intermediate image plane located just after the first beam splitter, after which the beam is collimated and sent vertically towards the moving mirror assembly which (for reasons discussed below) utilises roof top mirrors. The roof top shifts the beam and sends it up towards the camera mirror. Symmetrical with the collimator, the camera focuses the beam to an image plane just before the output beam splitter. The output relay mirror focuses the beam onto the detector arrays. To accommodate the components within the available volume, a fold mirror is needed to take the beam out of the plane again. This configuration allows a single mirror mechanism to be employed for both arms of the interferometer and achieves a folding of a factor of four in the optical path difference with respect to the actual movement of the mirrors. The second input port of the interferometer is used for a calibration source – the nature and use of this source is discussed in section 3.

All the optical components except for the final filters, lenses and the detector assemblies will be mounted from the common optical bench at a temperature of <5 K. The detectors, lenses and final optical filters are mounted in a thermally isolated

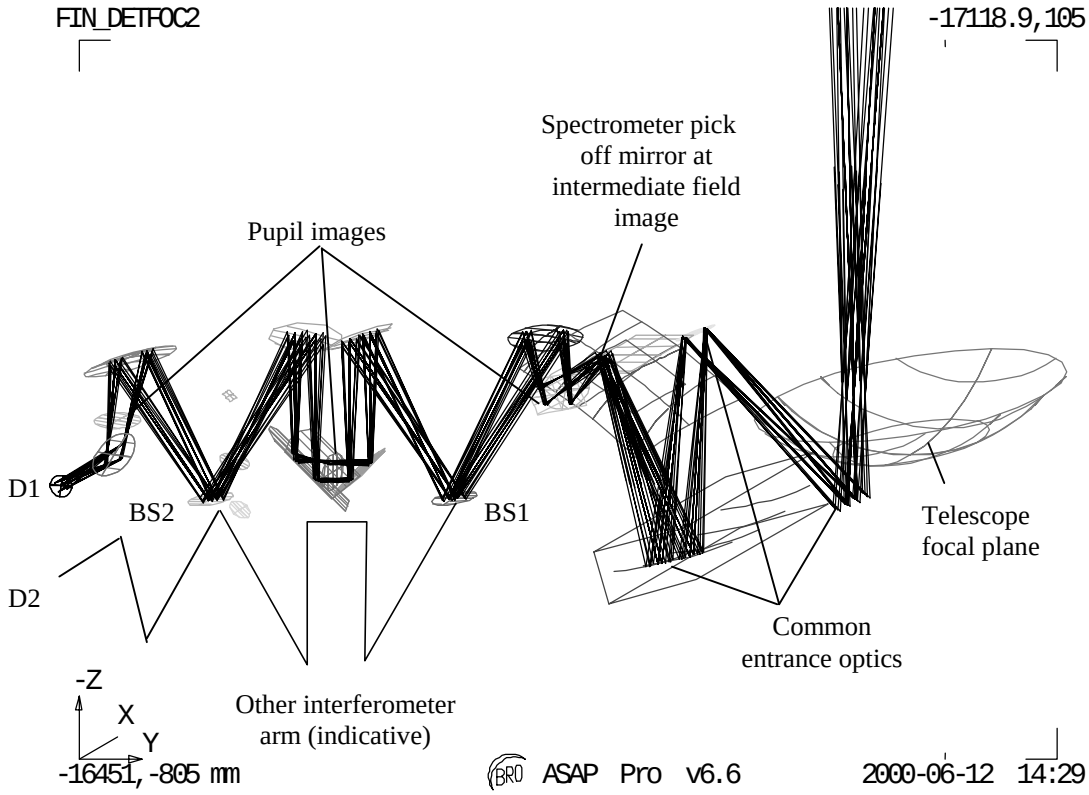

Figure 1: The outline optical design of the SPIRE FTS: the concept is based on a Mach-Zehnder interferometer with its arms folded in order to avoid beam shearing during scanning of the optical path difference twin intensity and uses dividing beamsplitters (BS1 and BS2). There are two separate detector channels (D1 and D2) only one is shown here, the other is in the symmetric arm of the interferometer shown indicatively. The folding allows the optical path of both arms to be changed simultaneously with a single scanning mechanism, hence doubling the available resolving power for a given movement of the mirror mechanism. Roof top mirrors are used within the mirror mechanism

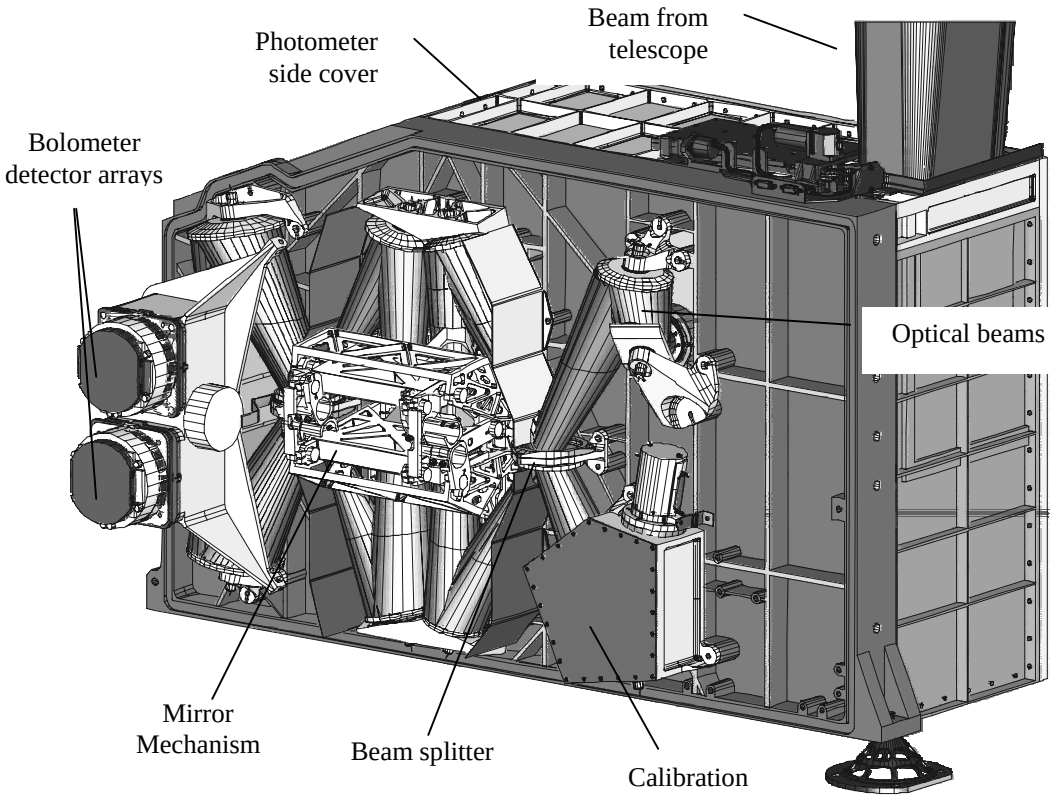

Figure 2: View of the spectrometer side of the SPIRE instrument with the spectrometer side outer cover removed. The optical beam from the telescope is refocused by three common mirrors on the photometer side of the instrument to an intermediate field image where the field for the spectrometer is picked off (see figure 1). The beam passes through the optical bench into the spectrometer.

box strapped to the Herschel cryostat liquid helium tank at <2 K. Pupil images are located at three positions in each arm of the interferometer. One between the pick off mirror and the first fold mirror is used as the limiting exit pupil for the spectrometer part of the instrument because its image does not shear with respect to the telescope secondary which is the final limiting aperture stop in the system. A second pupil image is placed, naturally, in the centre of the collimated section and a third between the final fold mirror and final image plane. This third pupil is used to control unwanted rays from entering the detector. The actual position of the pupil image is not mechanically accessible so the final fold mirror is used as a reflective stop instead with a black surface around the mirror surface defining the shape of the aperture. This final aperture stop is slightly oversized compared to the geometrical image of the pupil to allow for some beam wander for off axis positions in the field. The exit aperture stop is sized to the geometric size of the pupil image therefore clipping a single mode Gaussian beam from the feedhorn arrays at $1/e^2$ of the intensity profile (see reference 6 for more details).
In order to control the out of band radiation entering the instrument, filters will be placed at the entrance to the common optics box; at the first pupil image at <5 K; at the entrance to <2 K enclosure and finally band limiting filters will be placed directly in front of the bolometer arrays at 300 mK. The beam splitters themselves will also have some limited out of band rejection capabilities.

A consequence of the very limited space available for the spectrometer is that it has not proved possible to make the final beams onto the detectors telecentric. This would not be a problem except that the detectors use feedhorns and, because of the detector construction, these need to be on a flat focal plane. The beam from the off axis detectors therefore “misses” the image of the final pupil and there is a loss of efficiency. The problem is exacerbated when the optical path difference is changed as the interfering beams will shear past each other leading to loss in fringe contrast. In order to solve this problem a lens has been added to the detector assembly that moves the pupil image effectively to infinity and makes the optics appear

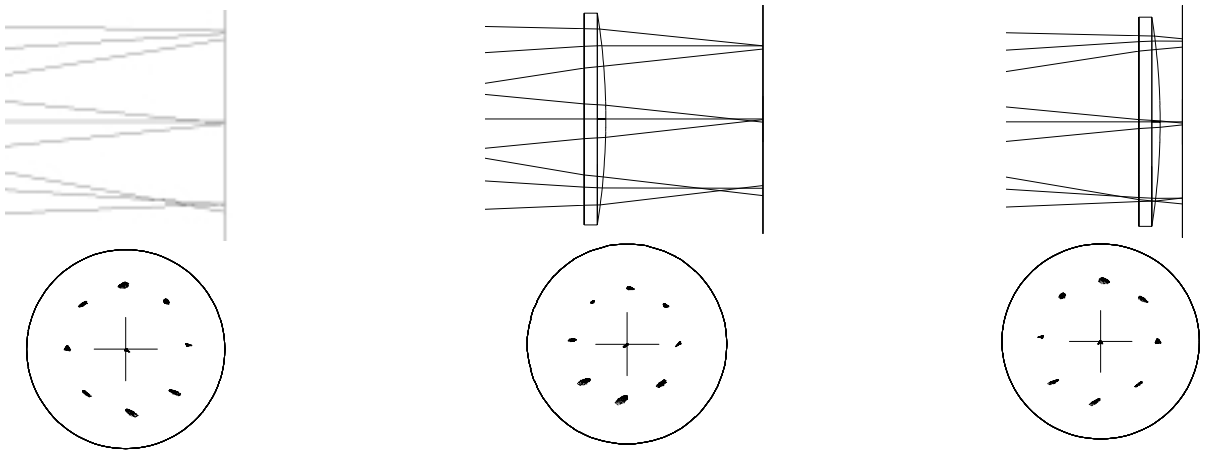

Figure 3: Three panels showing the effect of adding a lens in front of the feed horn arrays. On the left the on-axis and extreme off axis rays are shown as in the original optical design. The non-telecentricity of the design is shown by the angles of the off axis central rays. The imaging performance is shown in the lower part of the panel. The effect of the lenses on the short and longwavelength arrays is shown in the other two panels. The off axis rays are now parallel as they reach the detectors arrays – i.e. they appear to come from a point at infinity. The mechanical constraints on the placement of the lenses means that the shortwavelength array lens is not as close to the focal plane as desirable and there is a slight loss in image quality in the this band.

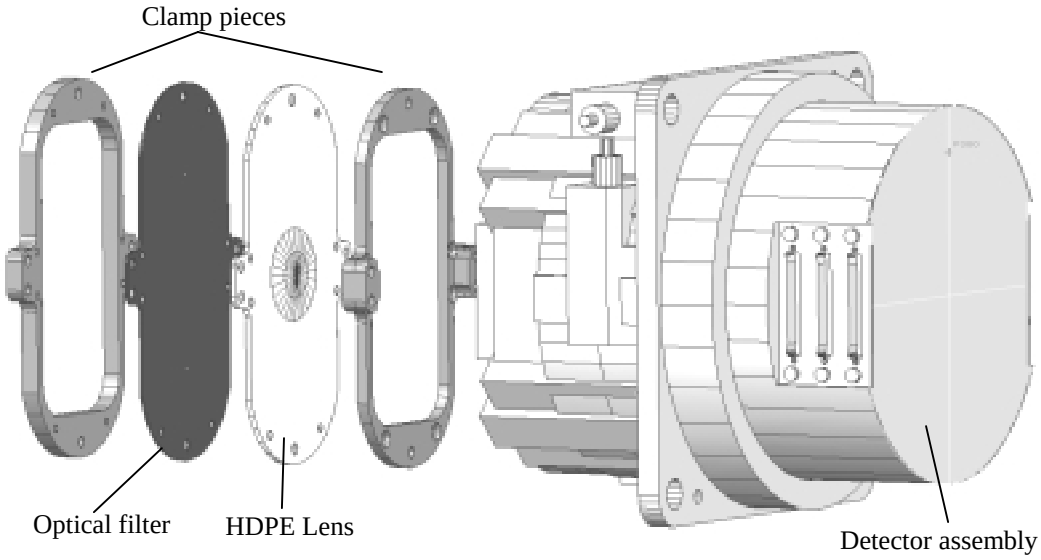

Figure 4: Mechanical implementation of the lenses in the spectrometer detector assemblies.

telecentric to the detectors. Figure 3 shows the effect of adding this lens on the final beams and the imaging performance of the two detector bands. The lens will be made from high-density polyethylene (HDPE) and there will be a small (few percent) loss in overall transmission efficiency of the instrument. Also, because the lens is not precisely located at the focal plane, there will be an additional reduction in the Strehl ratio. Figure 4 shows how the lens will be implemented in the detector assemblies.

A further change in the optical design of the spectrometer compared to that reported in reference 4 is the use of roof top mirrors in the moving mirror mechanism rather than corner cubes. The original intention was to use corner cubes as these gave immunity from rotation and translation errors in the mirror movement – i.e. if the mirror movement is not perfectly parallel to the optical axis the fringe contrast would be reduced by beam shear. However, the use of corner cubes at this

point in the optical chain also caused the image to be rotated with respect to the co-ordinate system defined by the instrument optical axis and the orientation of the orthogonal movements of the beam steering mechanism – the so called chop and jiggle axes. One of the methods of reducing the influence of errors in the mechanism speed control (see below) is to use the instrument in "step-and-look" mode rather than "scan" mode. In step-and-look mode the mirror mechanism is stopped at each sample interval and the beam steering mechanism is used to chop the signal between source and background. In order to make this operation efficient it is necessary to have the arrays aligned with the chop axis. Given that the corner cubes rotate the chop axis with respect to the array alignment, it is necessary either to rotate the arrays in the same sense, or to replace the corner cubes with roof tops which do not rotate the axes. The limited space available for the arrays meant that rotating them was not possible, therefore roof tops are baselined for the mirror mechanism. This decision means that the spectrometer performance becomes sensitive to tilt errors in the mirror movement. However, the requirements on the mirror tilt are not severe (<1 arcmin over the full movement range to preserve fringe contrast >80%) and well within the capabilities of the present mechanism design.

3. IMPLEMENTATION OF THE SPIRE FTS

The SPIRE FTS consists of the optics, as discussed above; the detector arrays, as discussed in reference 3; the mirror mechanism, together with its drive electronics, and a calibration system (discussed in detail in reference 7). The designs for these last two items are discussed in this section. In particular the flight design for the mirror mechanism and the method of position measurement employed are described, as it is these that will largely determine the final performance achievable with the instrument.

3.1 MIRROR MECHANISM

In order to achieve the required maximum spectral resolution (0.04 cm^{-1}) a change in optical path difference of about 12.5 cm is required. The optical design folds the beams such that the actual mirror travel required is ¼ of this. For the sake of observing efficiency it is expected that the highest resolution interferograms will be taken single sided and only observations with resolution <0.4 cm^{-1} will be taken double sided. The requirements on the mirror mechanism are therefore for a movement of –3.2 to 32 mm with a linear trajectory aligned in the SPIRE structure with respect to the optical path position. The mechanism must also scan at a constant speed in the range 0.2 to 1 mm/s with a 10 µm/s RMS stability. This must be achieved at least in a +/- 3.2 mm travel sub range around the Zero Path Difference (ZPD).

In order to allow correct sampling of the detector signals the position measurement system must be able to output the positions along its travel at a frequency up to 250 Hz with a 0.1µm relative precision in the +/- 3.2mm sub travel range, and

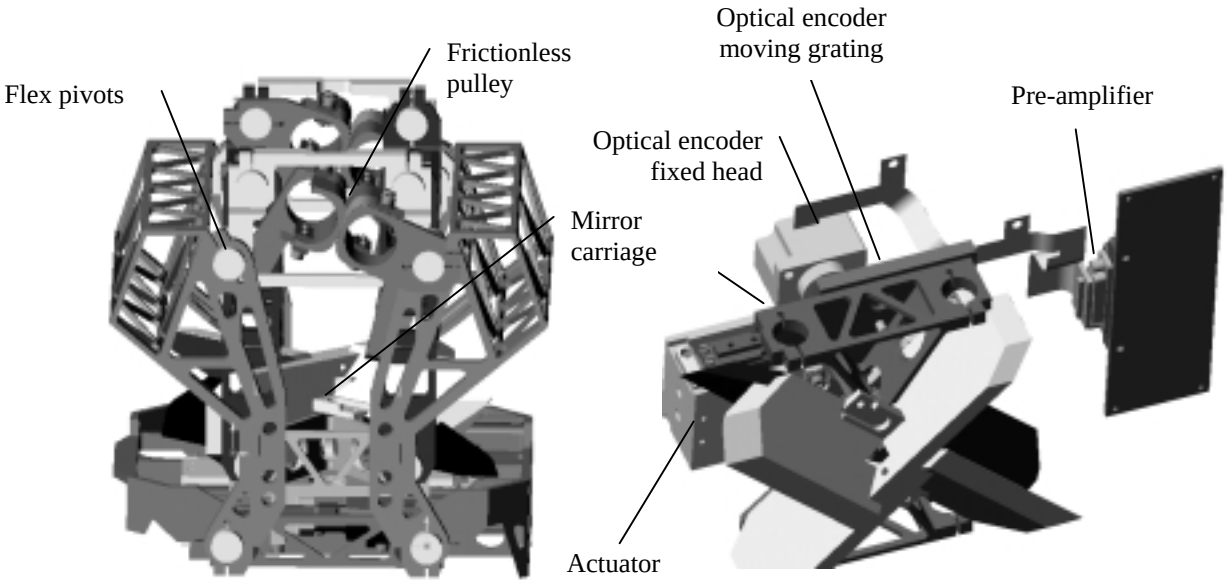

Figure 5: Two views of the flight design of the mirror drive mechanism. On the left the complete assembly is shown with the flex pivots and frictionless pulley system. On the right the upper structure is removed to show the optical encoder and linear actuator positions.

a 0.3 μm relative precision elsewhere.

To meet these requirements, the mirror movement in the FTS is effected using a double parallelogram mechanism developed and prototyped at Goddard Space Flight Centre (GSFC) - see reference 4 and section 4 of this paper. The prototype design proved not to be stiff enough to withstand the launch vibration environment and the flight design of the mechanism (figure 5) has had to be substantially stiffened to move the structural natural frequency above 170 Hz to avoid the natural frequency of the SPIRE instrument itself. The girder type structures that connect the two arms of each moving section are designed to make the assembled structure resistant to twisting about the vertical axis. As well as avoiding problems with launch loads this stiffening prevents parasitic modes in the structure that are not "sensed" by the position measurement systems and are therefore not well corrected for by the control electronics. Such parasitic vibrations could be induced from other mechanism within the spacecraft system such as the reaction wheels for attitude control.

3.2 POSITION MEASUREMENT SYSTEM

The basic position measurement of the mirrors is carried out using a modified Heidenhain LIP401A optical encoder[8]. These devices use interference from between the diffracted orders from a moving and a fixed grating to produce modulated signals in three separate detectors as one grating is moved with respect to the other. The signals seen in the detectors are approximately 120°-phase shifted with respect to each other. These are then converted electronically into the two 90° phase-shifted signals that are characteristic of Heidenhain encoders. The basic step size of the LIP401A is 2 μm with a measurement accuracy of 2.6 nm as supplied. After modification and with cryogenic operation an accuracy of 10 nm has been achieved.

The commercial devices have been extensively tested for their compatibility with cryogenic operation. Several modifications are necessary to the commercial devices to allow their use in a space experiment and at cryogenic temperatures.

- Neither the commercial LED nor the photodiodes provided are suitable for space applications. Hammatsu S2386-18K silicon photodiodes will be used for the detectors and a GaAlAs type OD-880W LED will be fitted. The LED and detectors will be fully cold redundant in the flight system – this means the Heidenhain provided focal plane has been replaced by a custom built one containing two LEDs and six photodiodes.

- The scanning grating and the fixed grating must be made of the same material to avoid problems with the change in size as the system is cooled down. For the flight system both will be made from ZeroDur

- The fixed grating in the optical head was found to be "squeezed" by its mounting when cooled down. This causes a distortion of the grating leading to a severe loss of contrast in the modulated signal. This was cured by machining slots in the mount to provide stress relief when the unit was cooled.

- A preamplifier is required for the photodiodes. This must be as close a possible to the optical head. In the flight unit a MOSFET preamplifier will be used mounted in the body of the mechanism structure as shown in figure 5.

A disadvantage of the optical encoder is that it gives only a relative position. The system must count steps from some fiducial mark in order to reconstruct the absolute position of the mirrors. The system of providing this fiducial mark in the commercial encoders is not suitable for space use. Instead 2 linear-voltage displacement transducers (LVDT's) - one nominal and one redundant – have been added to the system to measure the absolute position close to the ZPD. They are the Schaevitz MHR100 type with an accuracy of 100 nm over a movement range of ± 3.2 mm.

3.3 THE CALIBRATION SYSTEM

The second input port of the FTS is used to provide a calibration source; this source serves a number of functions. The first, and most basic, is to provide a direct photometric calibration for the astronomical signals. This will be achieved by careful comparison of the signal from the calibration unit to an accurately calibrated source during ground testing of the instrument before launch. The advantage of a double port interferometer such as this is that this calibration signal can be present during the entire period of measurement. This means that changes in performance of the system can be readily removed from the data during ground processing. The downside to this is that the photon noise is increased – see section 5 for a discussion of this effect.

The second use of the calibrator is that it can be used to null the continuum radiation from the warm telescope that is constantly present in the SPIRE beam because it is 90 degrees out of phase with the primary input port. There are two important reasons for wishing to do this:

1. It reduces the dynamic range of the signals close to the ZPD. This is required because otherwise digitisation noise from the electronics would begin to become a problem.

2. The effects of scan speed variation on the noise in the measured spectrum are directly related to the slope of signal at any point in the interferograms (see discussion below). Except when observing very bright astronomical sources, most of the signal at or close to the ZPD will be due to the telescope background. Noise in measuring this signal will prevent accurate narrow band photometry of the faint astronomical sources of interest.

The design of the calibration unit is described in detail in reference 7. In brief it consists of four small black plates thermally isolated from the main SPIRE structure. Two of these plates can be operated at one time (for redundancy) and each can be separately controlled to a given temperature. The plates are 3 mm and 5 mm diameter respectively. Because the calibrator is placed at an image of the telescope pupil radiation from the heated plates reaches all detectors in the field of view. The diluted 80-K spectrum from the Herschel telescope is, in principle, matched by using only a part of the total area of the pupil image as an emitting surface. By having plates of different diameters and independently heated it will be possible to match the spectrum of the telescope emission across the whole of the detection band simultaneously.

3.4 DRIVE ELECTRONICS

A single electronics unit, the Mechanism Control Unit (MCU), will be used to control the movement of both the FTS mirror mechanism and the Beam Steering Mirror (BSM). The block diagram for the unit is shown in figure 6. The unit is comprised of three basic parts: the Multi-Axis Control card (or MAC) and two signal conditioning cards, one for the BSM and one for the FTS mechanism. The control of the mechanism movement is carried out using a Temic DSP 21020 chip. The algorithms are based on trajectory generators and digital PID controllers associated with filtering for notching of mechanism modes. The control parameters are held in memory and can be altered by means of commands sent to the unit via the spacecraft command and data handling system and the SPIRE on board computer; which deals with high level control and data handling for the instrument. The same system is used to command the operation of the mechanisms, such as commanding a given position of the BSM; ordering the FTS mechanism to its “home position” or determining the speed of the FTS mirror motion.

The DSP software is based on a master scheduler on the principle of time sharing without the use of a specific multitask kernel. The tasks to be performed are called on by a software interrupt generated by the inner DSP timer. The software interrupt defines the global sampling time (i.e. the computation cycle) of the DSP tasks at a programmable rate between 100 us min and 300 us max At each cycle the following tasks are performed :

- the FTS mechanism control loop task
- the BSM chop axis control loop task,
- the BSM jiggle axis control loop task,
- the communication with the command line and other various internal DSP tasks
- data packet assembly and transmission to high rate serial link to the SPIRE on-board computer

In addition to the DSP an ACTEL FPGA is used for internal data bus control; interfacing with the amplifier DACs; interfacing with the multiplexed ADC; digital inputs and outputs towards the mechanism control boards and the optical encoder pulse counting and logic. The same FPGA is used for the low level protocol handling on the serial links with the SPIRE on-board computer.

There are two methods of determining the position of the FTS mechanism using the optical encoder. The more crude method is to detect the zero crossing points of the sine and cosine signals from the encoder detectors in analogue electronics and use these to generate pulses that can be counted by the digital part of the system. This gives mechanism “steps” that are 2 μm apart and the time between these pulses is measured using the internal clock. This method of position determination is used to determine the length of the mirror travel and can be used to position the mirrors when in step and look mode. The time between pulses can also be used to determine the average velocity between pulses. However, the zero crossing determination is not accurate enough to give the fine control required on the speed of the mirrors when using scan mode. Instead the signals are digitised via the ADC and read directly into the DSP control algorithm. The position is determined

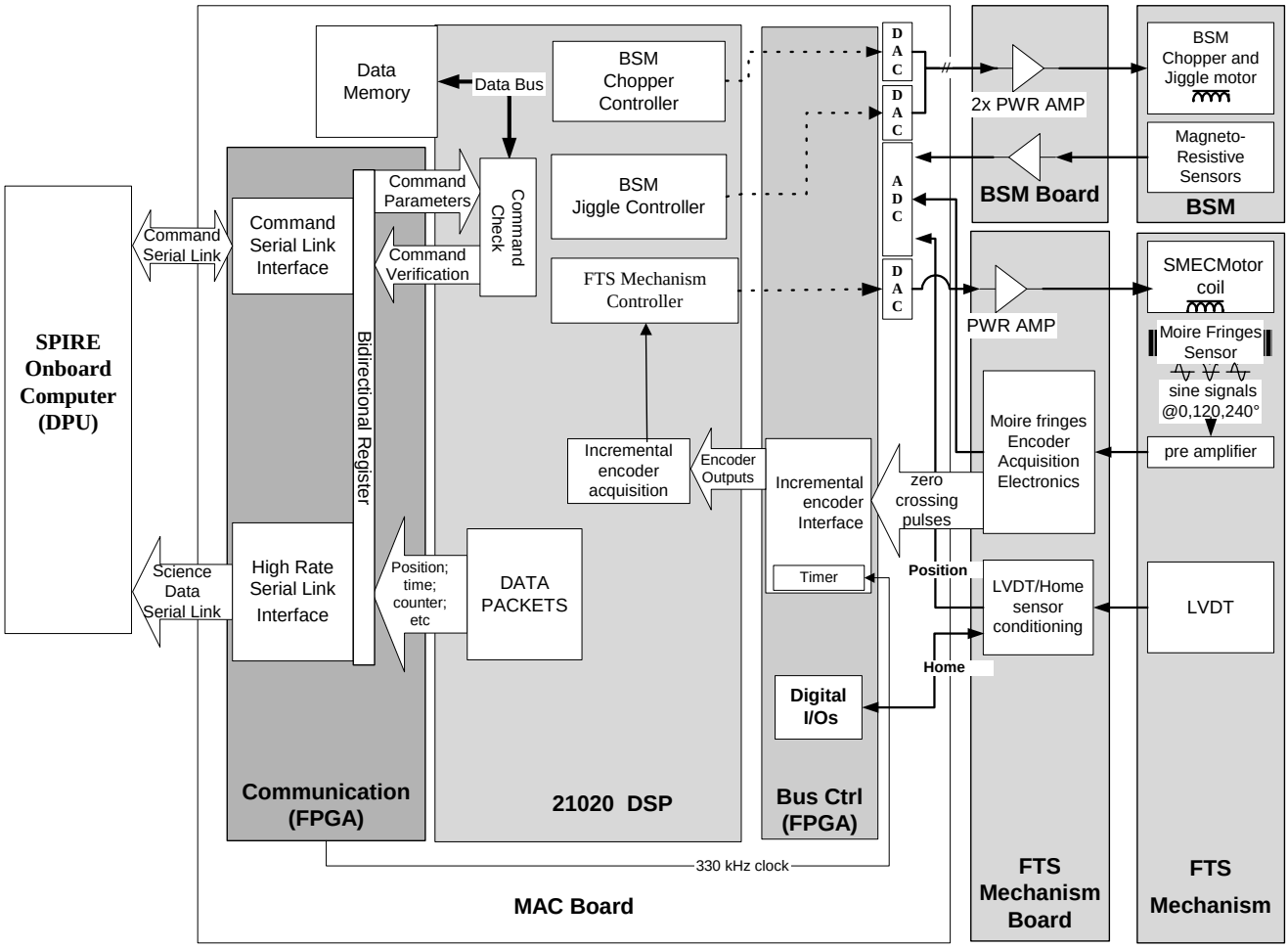

Figure 6: Block diagram of the drive electronics for the SPIRE mechanisms

much more accurately by computing the arctangent from the three sinusoidal signals from the detectors. This position is used in the feedback loop to the drive current of the actuator to control the speed of the mirrors during scanning. The absolute position of the mirrors can be determined from the LVDT signals within a limited range of movement of the mirrors. In the event of a failure of the optical encoder the LVDT signals can be used for speed control. The zero point of the LVDT output is designated as the "home" position of the mirrors and is sensed via analogue electronics and converted to a pulse read directly by the FPGA. This allows simple operation of the mechanism by giving the ability to always command the mirrors to a known absolute position within the movement range; the scan start position and scan length can then be determined by counting encoder step pulses from this home position.

4. PROTOTYPE TESTING

Two prototype mechanisms have been built by GSFC. The first of these[4] had the actuator placed on top of mirror platform and was not a suitable design for flight. The second, shown in figure 7 on an optical test set up described below, had the actuator underneath and was much more like the design to be implemented for SPIRE. Both these prototypes have been used to evaluate the control algorithms required to be implemented in the flight electronics. A dSpace[9] simulation system was used in conjunction with standard drive amplifiers for the actuators and a DSP test board to evaluate the performance of the prototypes and the methods required for the control of the speed. Figure 8 shows the recorded response of the system in open loop control. The natural frequencies of the mechanism are clearly seen at about 50; 80; 130 and 200 Hz. A mathematical model was built of the system response and used to determine the optimum notch filtering to apply in the control loop to avoid driving the system at these resonant frequencies.

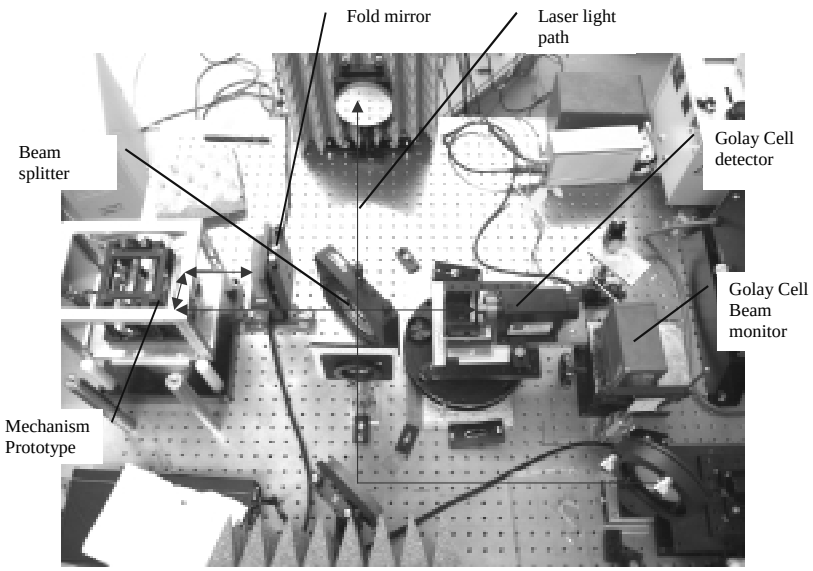

Figure 7: Experimental set up for testing the prototype mechanism using a far infrared laser.

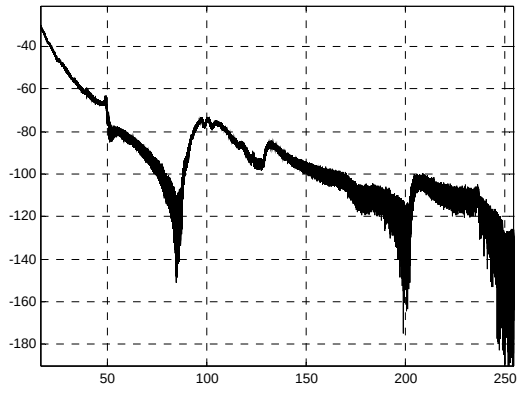

Figure 8: Response of the prototype mechanism to mechanical stimulation as a function of frequency. The mechanical resonances show up as sharp breaks in the power spectrum

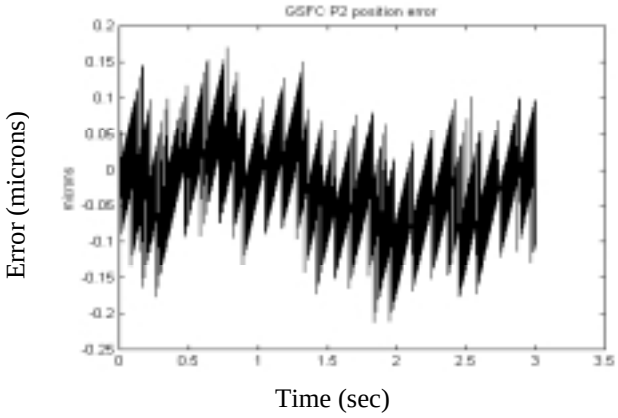

Figure 9: Position error versus time for the prototype mechanism depicted in figure 7 controlled with breadboard drive electronics at a scan speed of 500 μm /s.

The algorithm was run on the prototype set up and the speed and position errors recorded. The recovered position errors, determined by comparing the actual position at a given time with that calculated from the average velocity and the time at which the position was passed, are shown in figure 9 with the mechanism driven at the nominal 500 μm/second. This position error is recorded un-filtered.

In order to determine the effect of the errors in scan control on the performance of the spectrometer, an optical test was set up using an Edinburgh Instruments Far Infrared Laser. The test set up is shown in figure 7. The beam from the laser was not collimated other than by the natural collimation from the laser cavity, therefore the beam diverged somewhat as it went through the interferometer. This caused problems with extra reflections as discussed below. The path through the interferometer was essentially the same as through the SPIRE design except using a single beam splitter and the mechanism movement gave the same factor of four change optical path difference. The Golay cell and amplification chain had a single RC type time constant of 7.7 Hz and the signal was recorded asynchronously with the mechanism position data as the

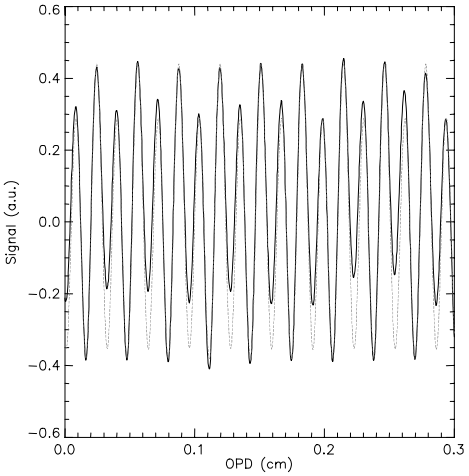

Figure 10: Portion of the recorded signal (dark solid line) from the prototype test with an FIR laser. The interferogram has been fitted as described in the text. The fit is shown as the dotted line.

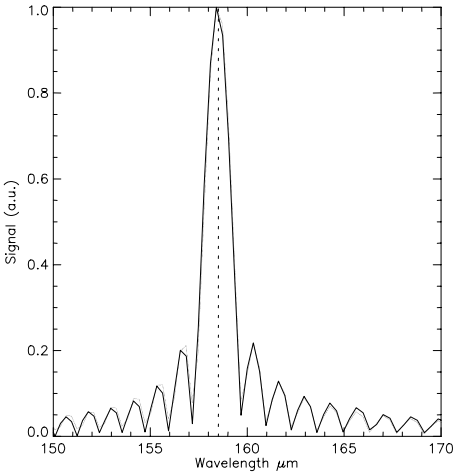

Figure 11: Data from figure 10 transformed to the spectral domain. The fitted line is shown here but cannot be distinguished from the data. The laser line wavelength is shown as the dotted vertical line.

mechanism was scanned at approximately 500 μm/s. This replicates the method of operation that will be employed in SPIRE except that the SPIRE detectors will have rather faster time constants at about 20-25 Hz. The recorded interferogram for a laser line at 158.513 μm (63.0861 cm^{-1}) is shown in figure 10 and the recovered line spectrum in figure 11. Note in the interferogram two frequencies are present – this is due to a parasitic reflection from the mechanism structure giving an interference at half the OPD of the main interference from the corner cube mirror. The interferogram was fitted by constructing two cosine functions of the optical path difference:

$$I = A\cos((2.0\pi\sigma)(4x) + \pi/2.0 + \delta\phi) + B\cos((2.0\pi\sigma)(2x) + \pi/2.0)$$

Here σ = 63.0861 cm^{-1} and x is the distance the mirror actually travels. The phase shift of $\pi/2$ is necessary to synchronise with the actual signal and A,B and $\delta\phi$ are variables to be fitted to allow for intensity and phase shifts between the two frequencies. The intensities of the two components were adjusted incrementally and the co-added signal was filtered by the detector and amplifier response to get an eyeball fit to the data shown in figures 10 and 11. We can see here that the line is perfectly recovered and that, for narrow line spectroscopy at least, the influence of the position errors and scan speed jitter is minimal. The situation is rather different when measuring continuum radiation and this is discussed in the next section.

5. PERFORMANCE SIMULATIONS

The influence of position error, and to some extent velocity error, on an interferogram of a monochromatic line can be understood in general terms from standard error analysis starting from the relationship between signal, OPD, velocity and frequency. That is, for velocity errors at a given frequency one expects to see ghost lines displaced from the main line at the frequency of the velocity error. Also one generally expects the errors in the interferogram to be proportional to the differential of the signal with respect to OPD. When the situation becomes more complex, with a spectral distribution of velocity errors and a continuum input spectrum, the straightforward error analysis is no longer sufficient to describe the problem. Instead a Monte Carlo model has been written in IDL[10] as described in reference 4.

The model has been extended to allow the measured spectrum of position errors for the prototype mechanism to be used to envelope the randomly generated velocity noise. An array of times at which each encoder position is passed is generated using the random errors in velocity in parallel with an independently fixed time sampled signal array generated from the cosine transformation of an input spectrum. The point here is to replicate the actual asynchronous manner in which the SPIRE FTS will be operated. That is any velocity errors, combined with any inaccuracy in the mechanism position sampling, will cause the signal at a given fixed time to be in advance or behind where the mechanism position calculated assuming a stable velocity expects it to be. The encoder position times are highly over sampled whilst the signal sampling

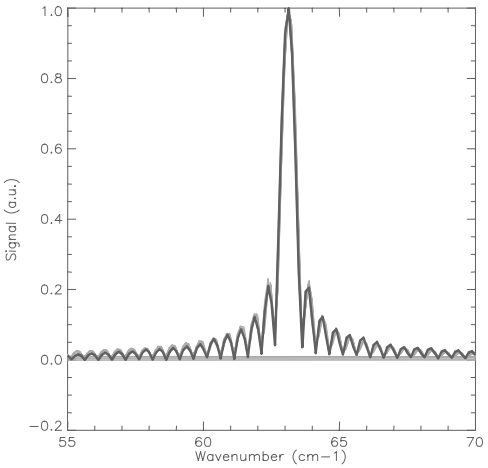

Figure 12: Simulation results for the 158.513 μm line used in the prototype tests. The data from the tests are the dark line and ten simulated spectra are shown as light grey.

is at four times the required Nyquist rate for the speed of the mirrors. The actual position of the mirror at the fixed signal sample times is then interpolated from the calculated velocity at that time and the position array and interferogram used to transform the data into the spectral domain once more. To assess the impact on the noise in recovered spectrum, the model is run several times resetting the random array of velocity errors each time.

Figure 12 shows the results from the simulation compared to the data measured using the prototype mechanism and the laser. The results from the simulator using the same detector filtering characteristics agree well with the data. Although the noise in the measured data is difficult to assess, the noise spectrum in the simulation and that estimated from the difference between the theoretical prediction and the measurement (see figure 11) agree in form and to within a factor of 2 in level.

In the real observing situation, any astronomical spectrum is always seen on top of the emission from the warm Herschel telescope; this is assumed to be an 80 K black body with a 4% emissivity. To test the effect of the measured position noise spectrum from the prototype on a continuum spectrum, the program was run with the two optical bands of the SPIRE FTS and a continuum plus line spectrum together with an 80 K telescope. The calibration port of the FTS was simulated as having a black body source at 75 K – this compensates the signal at ZPD to 5% of that without the source. Figure 13 shows the results for the short wavelength band as a function of the mirror speed, given here as rate of change of OPD (v_{opd}). The effect of the compensation is clearly seen as the enhanced contrast of the line against the continuum from the telescope and the effect of increasing v_{opd} and the electrical filtering is seen as a reduction in the signal and a roll off of the spectrum.

A further test of the effect of the position noise and actual mirror velocity is shown in figure 14. Here the signal to noise across each band is plotted as a function of v_{opd} for the compensated and uncompensated cases. There are several points to note about this figure:

- The position noise is modelled as being independent of the mirror velocity – this is as observed with the prototype system. Thus all else being equal the faster the mirrors are scanned the better the S/N in the final spectrum
- This is always true for the lower frequency band where the detection frequencies are always well away from the electrical filtering

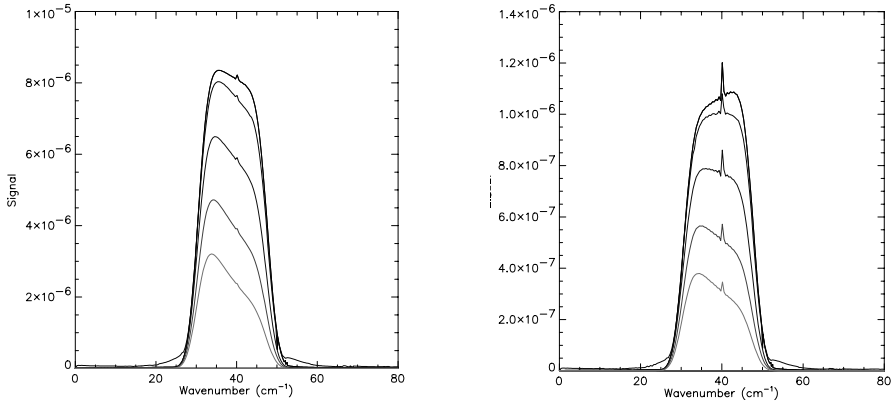

Figure 13: Simulation results for a continuum and line spectrum with uncompensated telescope background (left) and the same spectrum with 5% compensation of the telescope background (right). Here only the higher frequency band of the SPIRE FTS is modelled and the effect of increasing the speed of the mirrors is plotted with v_{opd} = 0.05, 0.1, 0.2, 0.3 and 0.4 cm/sec – upper to lower curve in each case.

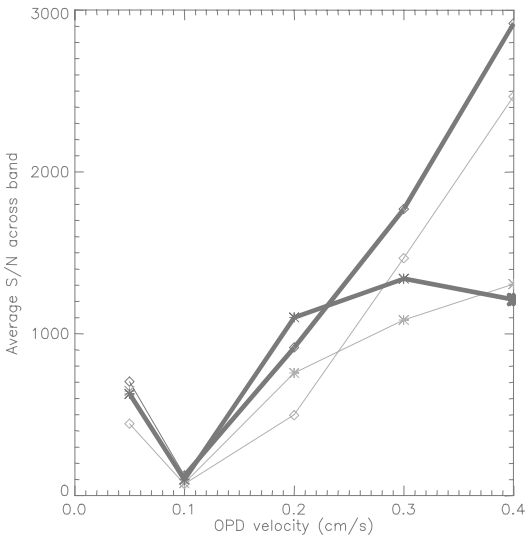

Figure 14: Average S/N across shortwavelength (stars) and longwavelength (diamonds) bands as a function of v_{opd} for compensated (light) and uncompensated (dark) telescope cases

- Using the calibration source to compensate the telescope background adds photon noise – as expected. However, no account is taken in this model of any problems that might occur with digitisation noise in the electronics due the large dynamic range required to measure the peak at the ZPD in the uncompensated case, or the beneficial effects of increased contrast of the line on the detectability of weak features in the spectrum.
- The break in the increase in the S/N curve in the higher frequency band occurs at about 0.2 cm/s for the electrical filter at 25 Hz and a 20 Hz 3 dB detector response. This is taken as the nominal operating point for the SPIRE mirror mechanism, equivalent to 500 μm/sec.

A prototype mechanism; position measurement and electronic control system for the SPIRE FTS has been built and tested using an FIR laser. The performance of the SPIRE FTS has been further evaluated using a sophisticated Monte Carlo simulation. The simulated performance shows that, in the limiting case of measuring a continuum source in scanning mode, the velocity noise will limit the achievable S/N to a few thousand. The flight design for the SPIRE mirror mechanism is expected to have a superior velocity error performance compared to the prototypes because it is very much stiffer. If higher signal to noise ratios are needed for individual observations the step and look mode of operation whereby the FTS mirror is held stationary while the object is chopped using the BSM, will remove the influence of velocity errors at the expense of a small loss in observing efficiency. The influence of velocity errors on the measurement of narrow lines has been shown to be negligible both by experiment and by simulation.

6. REFERENCES

1. Pilbratt, G., “Introduction to the Herschel Space Observatory”, SPIE paper 4850-87, these proceedings (2002)
2. Griffin, M.; Swinyard, B.; Vigroux, L. , “SPIRE: Herschel’s submillimeter camera and spectrometer”, SPIE paper 4850-100, these proceedings (2002)
3. Rownd, B.;Glenn, J.; Bock, J.; Chattopadhyay, G.; Griffin, M.,"Design and performance of feedhorn arrays coupled to submillimeter bolometers for the SPIRE instrument aboard the Herschel Space Observatory”, SPIE Paper 4855-08 Proc. Millimeter and Submillimeter Detectors for Astronomy, Hawaii, (2002)
4. Swinyard, B.; Ade, P; Griffin, M.; Dohlen, K; Baluteau, J-P; Pouliquen, D; Ferand, D.; Dargent, P.; Michel, G.; Martignac, J.; Rodriguez, L.; Jennings, D.; Caldwell, M.; Richards, A.; Hamilton, P.; Naylor, D.; “FIRST-SPIRE spectrometer: a novel imaging FTS for the submillimeter”, Proc. SPIE Vol. 4013, p. 196-207, UV, Optical, and IR Space Telescopes and Instruments, James B. Breckinridge; Peter Jakobsen; Eds.
5. Dohlen, K.; Origné, A.; Pouliquen, D.; Swinyard, B., “Optical design of the SPIRE instrument for FIRST”, Proc. SPIE Vol. 4013, p. 119-128, UV, Optical, and IR Space Telescopes and Instruments, James B. Breckinridge; Peter Jakobsen; Eds.
6. Caldwell, M.; Swinyard, B.;Richards, A., “Beam pattern (diffraction) aspects in design of the SPIRE instrument”, Proc. SPIE Vol. 4013, p. 210-220, UV, Optical, and IR Space Telescopes and Instruments, James B. Breckinridge; Peter Jakobsen; Eds.
7. Hargrave, P.; Beeman, J.; Collins P.; Didschuns , I.; Griffin, M.; Kiernan, B.; Pisano, G.; Hermoso, R.; “In Flight Calibration Sources for Herschel-SPIRE”, SPIE paper 4850-94, these proceedings (2002)
8. *Exposed linear encoders*, http://www.heidenhain.com/Products/ExposedLinear/lip.htm
9. *Dspace Gmbh*, http://www.dspaceinc.com
10. *Interactive Data Language*, Research Systems Inc., http://www.rsinc.com